Geophysical Research Letters

RESEARCH LETTER
10.1029/2022GL102195

Satellite Evidence for Glyoxal Depletion in Elevated Fire Plumes

C. Lerot[1], J.-F. Müller[1], N. Theys[1], I. De Smedt[1], T. Stavrakou[1], and M. Van Roozendael[1]

[1]Royal Belgian Institute for Space Aeronomy, Brussels, Belgium

Key Points:

- Space observations of glyoxal-to-formaldehyde ratio typically show highest values near fires and decrease downwind
- A pronounced glyoxal depletion is identified above high-level pyrocumulonimbus clouds generated by intense wildfires
- Glyoxal depletion is likely due to retention in ice particles or outgassing as glyoxal hydrate when droplets reach the upper troposphere

Supporting Information:

Supporting Information may be found in the online version of this article.

Correspondence to:

C. Lerot,
christophe.lerot@aeronomie.be

Citation:

Lerot, C., Müller, J.-F., Theys, N., De Smedt, I., Stavrakou, T., & Van Roozendael, M. (2023). Satellite evidence for glyoxal depletion in elevated fire plumes. *Geophysical Research Letters*, *50*, e2022GL102195. https://doi.org/10.1029/2022GL102195

Received 22 NOV 2022
Accepted 5 FEB 2023

Author Contributions:

Conceptualization: C. Lerot, N. Theys
Data curation: I. De Smedt
Formal analysis: C. Lerot
Funding acquisition: M. Van Roozendael
Investigation: C. Lerot, J.-F. Müller, N. Theys, T. Stavrakou
Methodology: C. Lerot
Resources: C. Lerot, I. De Smedt
Supervision: N. Theys, M. Van Roozendael
Writing – original draft: C. Lerot, J.-F. Müller

Abstract Space-borne observations are used to characterize the fate of formaldehyde and glyoxal in wildfire plumes. Their distribution measured by the Tropospheric Monitoring Instrument reveals striking differences between the two compounds near intense fires. In typical situations, the glyoxal-to-formaldehyde ratio is highest near the fire (~0.1) and decreases downwind of the source area due to the larger contribution of pyrogenic emissions to the glyoxal abundance and to the longer lifetime of formaldehyde. However, a pronounced glyoxal depletion is detected above high-level clouds, not seen for formaldehyde, likely due to processing in pyrocumulonimbus clouds generated by the fires. This depletion suggests glyoxal retention upon droplet freezing and/or its outgassing in hydrated form in the upper troposphere. The absence of a sizable loss of formaldehyde during convection indicates that its hydration in liquid droplets and subsequent outgassing as methanediol represent at most a minor sink of formaldehyde.

Plain Language Summary Wildfires have a strong impact on air quality and climate owing to their associated large emissions of aerosols and gases. For very intense events, the injected material can reach high altitudes, in particular when the fires induce formation of convective pyrocumulonimbus clouds. Using the high spatial resolution observations from the spaceborne Tropospheric Monitoring Instrument, we investigate the respective distributions of formaldehyde and glyoxal, two proxys for volatile organic compounds emissions, at close proximity of intense fire sources. Typically, the glyoxal signal is maximum near the fire source and decreases downwind, while the formaldehyde distribution is more extended and shows weaker spatial gradient. However, we have identified a significant glyoxal depletion, not seen for formaldehyde, in case of injection at high altitudes, typically above the freezing level, suggesting its retention in ice particles or its outgassing in a hydrated form.

1. Introduction

Vegetation fires can have a very large impact not only on ecosystems but also on atmospheric composition and therefore on air quality (e.g., Voulgarakis & Field, 2015) with associated adverse consequences on health (Grant & Runkle, 2022). Fires directly emit large amounts of aerosols and gases, including carbon dioxide (CO_2), carbon monoxide (CO), nitrogen oxides (NO_x), volatile organic compounds (VOCs) and many other species. Subsequently, photochemical processing of these emissions often leads to enhanced levels of ozone and secondary organic aerosols (SOAs) (Majdi et al., 2019; Palm et al., 2020), thereby affecting the global radiative balance (Chang et al., 2021; Jiang et al., 2016). This environmental issue is becoming more acute as the intensity and frequency of wildfires are increasing due to hotter and drier conditions (di Virgilio et al., 2019; Pausas & Keeley, 2021; Senande-Rivera et al., 2022; Xu et al., 2020). Furthermore, the large number of megafires injecting material in the upper layers of the atmosphere raises concerns on their impact on the stratospheric composition and the ozone layer in particular (Das et al., 2021; Schwartz et al., 2020; Solomon et al., 2022).

Satellite measurements provide invaluable information on the global distribution of atmospheric trace gases and aerosols on a daily basis. Therefore, they are well-suited to characterize the spatial and temporal evolution of biomass burning plumes. In this context, the Tropospheric Monitoring Instrument (TROPOMI) in operation since October 2017 on board of the Sentinel-5 precursor platform (Veefkind et al., 2012) is of particular interest as it allows measuring column densities of a suite of key trace gases present during fire events, such as nitrogen dioxide (NO_2), carbon monoxide (CO), nitrous acid (HONO), formaldehyde (HCHO), glyoxal (CHOCHO), in addition to the absorbing aerosol index (AAI) (e.g., Alvarado et al., 2020; Theys et al., 2020; van der Velde, van der Werf, Houweling, Eskes, et al., 2021; van der Velde, van der Werf, Houweling, Maasakkers, et al., 2021). Compared to past atmospheric composition instruments, the high spatial resolution and better signal-to-noise

Writing – review & editing: N. Theys, I. De Smedt, T. Stavrakou

ratio of TROPOMI provide an unprecedented capability to sample biomass burning plumes near the fires but also further downwind. The improved level of details allows to better track fire plumes and to detect more localized or weaker sources. For example, it has been recently shown that TROPOMI is able to detect short-lived species such as HONO in fresh wildfire plumes (Theys et al., 2020). So far, most fire-related studies based on TROPOMI observations were based on the aerosol, CO and NO_2 atmospheric data products, with a focus on inferring information on plume transport (Johnson et al., 2021), NO_x emissions and lifetime (Griffin et al., 2021; Jin et al., 2021), and on the impact of fires on the carbon cycle and the radiative budget (e.g., Byrne et al., 2021; Li et al., 2020; Magro et al., 2021; van der Velde, van der Werf, Houweling, Eskes, et al., 2021; van der Velde, van der Werf, Houweling, Maasakkers, et al., 2021). In contrast, little has been done to exploit the TROPOMI HCHO and CHOCHO observations in the context of fires, despite their potential to inform on VOC emissions (e.g., Cao et al., 2018; Fu et al., 2008; Stavrakou et al., 2009). In addition, the spaceborne observations of glyoxal have attracted special attention due to the potentially significant contribution of this compound to the production of SOA, for which large uncertainties exist as evidenced by the high disparity between the predictions of different model schemes (Miao et al., 2021; Oak et al., 2022; Pai et al., 2020). The high solubility of glyoxal in water indeed favors its uptake on aerosols and cloud droplets, followed by aqueous chemistry processes leading to SOA (Hallquist et al., 2009; Knote et al., 2014; Pennington et al., 2021; Volkamer et al., 2007). However, the SOA production yields from glyoxal depend strongly on the atmospheric conditions, such as salt and water concentrations and the nature of the ambient aerosols (Galloway et al., 2011; Knote et al., 2014; Li et al., 2016). In wildfire plumes, the SOA production from glyoxal is even more uncertain. In this context, the fine-scale distribution of glyoxal and other compounds in and around fire plumes as observed by TROPOMI might provide valuable insights to better understand the fate and role of fire-generated glyoxal in atmospheric chemistry.

To our knowledge, only one study (Alvarado et al., 2020) conducted a joint exploitation of TROPOMI glyoxal and formaldehyde data, aiming to investigate the long-range transport of fire plumes during the 2018 Canadian wildfires. They concluded that, provided the short lifetimes of those species, oxidation of longer-lived precursors within the fire plumes was necessary to explain the observed spatial patterns at long distances from the fire sources. Here, we systematically investigate the glyoxal signal observed by TROPOMI at close proximity of intense fire sources during the period July 2018–December 2021. We compare its spatial distribution to that of formaldehyde via the computation of glyoxal/formaldehyde ratio (R_{gf}), a metric often proposed to distinguish NMVOC emission type and highlight differences caused by their different production/destruction mechanisms (Kaiser et al., 2015; Vrekoussis et al., 2010). We find outstanding differences under specific conditions, namely for elevated plumes associated to megafires as detailed further below. In particular, northeastern Australia faced an exceptional 2019/2020 season of wildfires with an unprecedented burnt area estimated at about 7.2 Mha (Nolan et al., 2021). These fires produced enormous amounts of smoke, pollutants and aerosols, sometimes injected at very high altitudes, which favored their long range transport (Hirsch & Koren, 2021; Kloss et al., 2021; Ryan et al., 2021; van der Velde, van der Werf, Houweling, Eskes, et al., 2021; van der Velde, van der Werf, Houweling, Maasakkers, et al., 2021). This has been reinforced by the formation of a record-breaking number of Pyrocumulus (PyroCu) and Pyrocumulonimbus (PyroCb) clouds in late December 2019/early January 2020 (Nolan et al., 2021; Peterson et al., 2021). Those clouds are fire-induced and smoke-infused convective storms, and their composition is dominated by smoke particles (besides water). Although their exact formation processes are complex and remain uncertain (Fromm et al., 2022), their impact on the atmosphere can be significant as they lead to rapid vertical transport and are direct injection pathways of trace gases and aerosols into the upper atmosphere. For example, the 2019/2020 Australian fires-related emissions have perturbed the recovery of the Antarctic ozone hole (Damany-Pearce et al., 2022; Solomon et al., 2022).

In Section 2, we describe the TROPOMI observations and the different data sets used in this study; in Section 3, we present a detailed analysis of the glyoxal variability near the intense fire sources during specific events, and finally we generalize and discuss our results in Section 4.

2. TROPOMI Observations and Other Data Sets

TROPOMI is a push-broom nadir-viewing instrument measuring light backscattered and reflected by the atmosphere and the ground in the ultraviolet, visible and short-infrared spectral ranges. With a swath width of about 2,600 km, it covers the entire atmosphere on a daily basis with a equator crossing local time of 13:30 and a spatial resolution of 5.5×3.5 km^2 (7×3.5 km^2 before August 2019) (Veefkind et al., 2012). The exploitation of those

radiance measurements allows retrieving information on key atmospheric species such as NO_2, O_3, SO_2, CO, CH_4, HCHO, CHOCHO, aerosols, and clouds, all relevant to the monitoring of the ozone layer, air quality and climate studies.

In the context of fires, the spatial distributions of the different species probed by TROPOMI differ significantly since they have all different production mechanisms (direct emissions or secondary production processes) and different lifetimes. For example, the spatial extent of NO_2, directly emitted by fires, is much more limited than for other species like HCHO, largely produced via secondary processes, while CHOCHO generally shows an intermediate distribution extent, since it has both direct and secondary sources.

Here, we use TROPOMI measurements of CHOCHO supported by NO_2, HCHO, AAI data and cloud parameters for the period July 2018–December 2021. The operational NO_2 and HCHO products as well as the scientific CHOCHO product are generated using a Differential Optical Absorption Spectroscopy (DOAS) approach (Platt & Stutz, 2008). The latter consists in retrieving in an appropriate wavelength range a slant column density (SCD, the atmospheric concentrations integrated along the effective atmospheric light path), which is then converted into a vertical column density (VCD) (i.e., atmospheric concentrations integrated from the bottom to the top of the atmosphere) using radiative transfer modeling, generally carried out assuming aerosol-free conditions and by using a priori vertical distributions of the trace gases from global model simulations. Those assumptions are far from being verified for the particular conditions associated with intense fires, making the SCD to VCD conversion highly uncertain. For this reason, this study relies on the analysis of the slant column densities only.

The glyoxal SCDs are extracted from the TROPOMI product based on the exploitation of absorption bands in the visible spectral range (435–460 nm) (Lerot et al., 2021). Formaldehyde slant columns are derived in the UV range (328.5–359 nm) and extracted from the operational product (De Smedt et al., 2021). Since NO_2 absorbs in the UV and visible ranges, its absorption cross-sections need to be included in the spectral fits of both HCHO and CHOCHO products. NO_2 slant columns are consequently available from those two products with systematic differences related to the different effective light paths in the respective spectral ranges. As suggested by Theys et al. (2020), this can be advantageously exploited to remove any bias in the R_{gf} values caused by radiative transfer differences between the UV and visible regions, including the effect of aerosols. To this end, R_{gf} is calculated as the CHOCHO/HCHO SCD ratio multiplied by the ratio of the NO_2 SCDs respectively fitted in the HCHO and CHOCHO fitting windows. This pragmatic approach assumes that the three gases have similar vertical distributions and requires large NO_2 columns to be accurate. These two assumptions are reasonable for freshly emitted plumes.

The TROPOMI AAI product is used here as a proxy for the presence of absorbing aerosols (Stein Zweers, 2022). In the following, we also use as proxy for the plume altitude an effective scene pressure provided by the O_2-O_2 cloud algorithm (Veefkind et al., 2016) and available in the latest version of the TROPOMI operational NO_2 product (van Geffen et al., 2022). In fire conditions with high aerosol loadings, discriminating clouds from aerosols is challenging and it has been shown that the effective scene pressure corresponds to the aerosol layer pressure (Wang et al., 2012). It has also been shown that the O_2-O_2 cloud product generated in the visible spectral range has an enhanced sensitivity for high aerosol loading cases compared to other products based on the O_2-A band in the near-infrared (Chimot et al., 2019). Finally, we use the Suomi-NPP Visible Infrared Imaging Radiometer Suite (VIIRS) Fire Radiative Power (FRP) product to locate and map the fire sources (Csiszar et al., 2014).

3. Glyoxal Variability Near Fire Sources

First, we examine the CHOCHO and HCHO spatial distributions for a typical case of intense fires without strong elevation of the plumes (effective scene pressures >500 hPa). Glyoxal signals measured during the 2019/2020 fire season in Southeastern Australia are often so strong that random uncertainties on the retrievals are not considered as a limiting factor for the interpretation of the data. Figure 1a shows enhanced glyoxal slant columns of up to 1.5×10^{16} mol.cm^{-2} near fire sources on 5 December 2019, well above the noise level of 6–10 $\times 10^{14}$ mol.cm^{-2} (Lerot et al., 2021). A strong reduction of the columns is observed downwind, as a result of atmospheric dispersion and physico-chemical destruction. As mentioned above, glyoxal and formaldehyde have relatively similar production mechanisms, namely, they are primarily formed from the chemical oxidation of NMVOCs, and they are also directly emitted by fires. The HCHO SCDs are also large ($\sim 4 \times 10^{16}$ mol.cm^{-2}) and have a larger spatial extent with a limited gradient downwind of the source area (Figure 1b). To further examine this aspect,

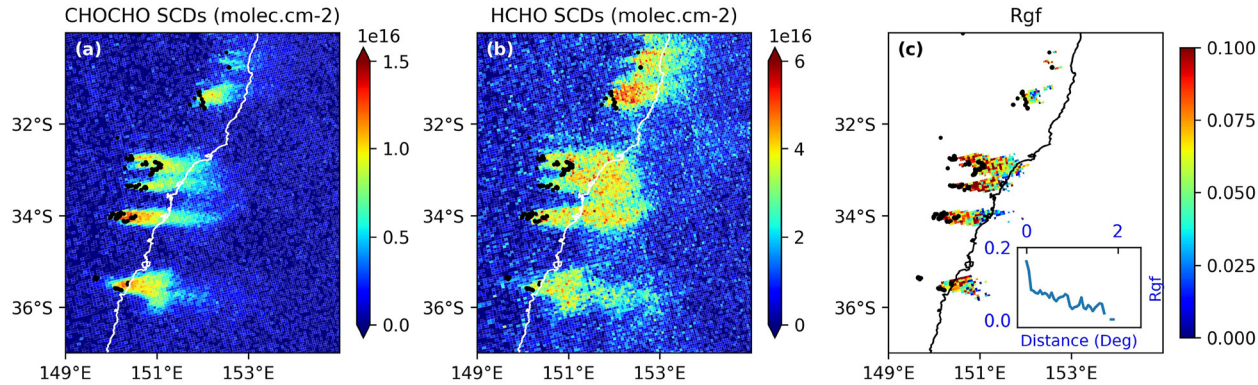

Figure 1. Spatial distribution of TROPOMI CHOCHO (a) and HCHO (b) SCDs observed on 5 December 2019 in Southeastern Australia. Panel (c) shows their ratio R_{gf} for scenes with AAI > 3 and NO_2 SCD > 1×10^{16} mol.cm^{-2} after correction for the different effective light paths in the UV and visible spectral ranges (see text). The inset figure depicts the R_{gf} as a function of the distance from the fire source. Fires with radiative power larger than 100 MW as detected by the Visible Infrared Imaging Radiometer Suite are indicated by the black dots.

the glyoxal/formaldehyde ratio (R_{gf}) is also displayed in Figure 1c. The large detected columns allow estimating reliably the R_{gf} values which, similarly to CHOCHO, decrease downwind, suggesting a larger contribution of direct pyrogenic emissions of glyoxal relative to formaldehyde (Fu et al., 2008; Stavrakou et al., 2009) and/or differences in chemical lifetime. This is even clearer in the inset panel showing the median R_{gf} as a function of the distance (i.e., the longitude difference in degrees) from the five mapped fire sources. The values of R_{gf} in the vicinity of the source are of the order of 0.1, in good agreement with previous studies (Alvarado et al., 2020; Chan Miller et al., 2014; Kluge et al., 2020; Zarzana et al., 2018). Consistently with Alvarado et al. (2020), our results show that R_{gf} decreases with the plume age, to values as low as 0.02 at a distance of about 200 km from the source area for this particular case.

Later during the 2019/2020 Australian fire season, an unprecedented number of PyroCb formed, in particular during 29–31 December 2019 and on 4 January 2020 (Peterson et al., 2021). For those fires, the R_{gf} displays a very different pattern. In Figure 2, we focus on the large-scale smoke plumes of 4 January as visible in the VIIRS/Suomi-NPP True color images (panel d). On that day, very large values of AAI were measured (>10, see panel e) and massive amounts of absorbing aerosols were injected at high altitudes in the atmosphere. Peterson et al. (2021) report that two PyroCb events injected particles up to about 16.5 km in the late afternoon of that day. O_2-O_2 effective scene pressures (panel f) derived from TROPOMI in the early afternoon, show several localized minima with values lower than 250 hPa, indicating PyroCb developments. The spatial distribution of R_{gf} (panel c) shows an unusual pattern with pronounced local minima co-located with the lower pressure scenes. As can be seen in panels a and b, the glyoxal SCD field also displays such local minima, while the HCHO spatial distribution shows little variation. Such behavior is unexpected given the high R_{gf} of fresh pyrogenic emissions (see discussion above). We have also examined the spatial distribution of SCDs of the other trace gases fitted simultaneously to glyoxal in the DOAS analysis. None of them shows spatial structures near the fire sources resembling those of glyoxal (see Figure S1 in Supporting Information S1). A spectral fit cross-correlation effect is thus unlikely. As mentioned above, R_{gf} is computed while taking into account the different effective light paths in the respective spectral ranges of HCHO and CHOCHO retrievals, thereby eliminating radiative transfer effects. A similar CHOCHO depletion has been observed for other elevated fire plumes in Australia (e.g., on 30–31 December 2019 and 5 March 2019) and in California during intense fire episodes with reported PyroCb formation (Lareau et al., 2022). This is illustrated in Figure S2 in Supporting Information S1 for the Creek fire of 5 September 2020. A decrease of the glyoxal SCD and R_{gf} values in excellent spatial correlation with the scenes with low effective pressures and high AAI is clearly observed.

4. Discussion and Outlook

In order to determine whether the identified CHOCHO depletion process occurs systematically for large fires, and under which conditions, we analyze all TROPOMI observations at the global scale from July 2018 to December 2021. We restrict the analysis to intense fires by requesting the NO_2 SCDs retrieved in the visible range to exceed

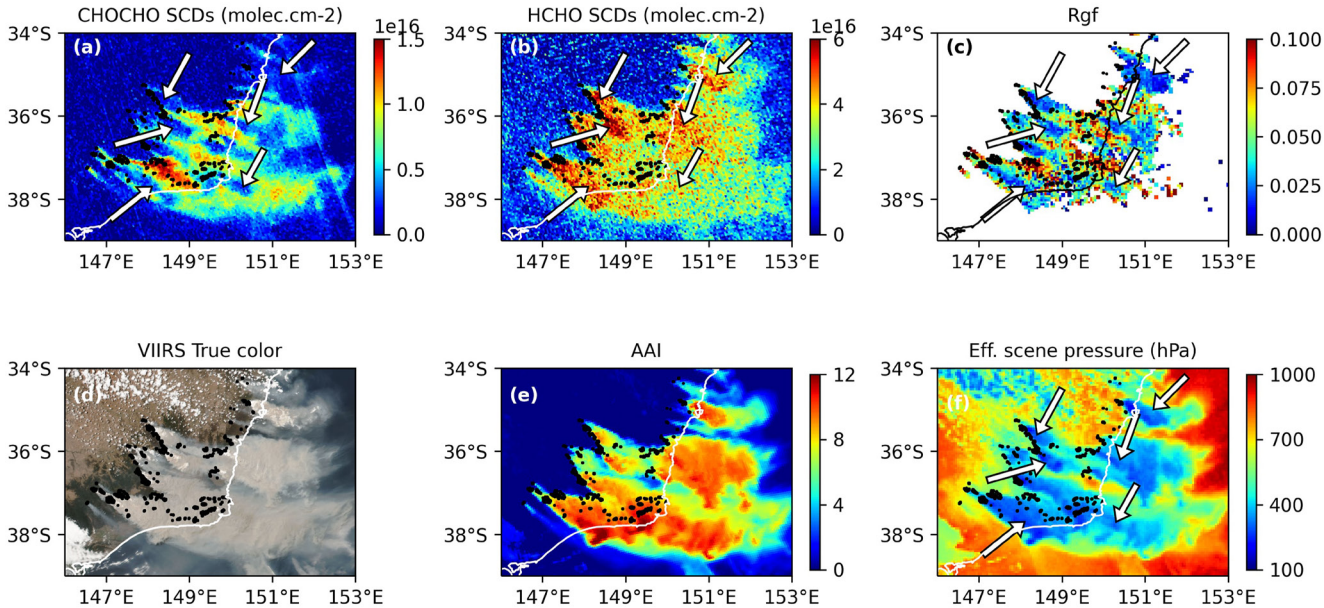

Figure 2. Spatial distribution of TROPOMI glyoxal (a) and formaldehyde (b) SCDs and their ratio R_{gf} for scenes with AAI > 3 and NO_2 SCD > 1×10^{16} mol.cm^{-2} (c) on 4 January 2020 in Southeastern Australia. Panels (d–f) showing the Visible Infrared Imaging Radiometer Suite (VIIRS) true color, and the TROPOMI absorbing aerosol index and effective scene pressures illustrate the presence of massive amounts of particles at high altitudes caused by the formation of several PyroCbs. The white arrows point to the locations where CHOCHO SCDs and R_{gf} minima are measured. Fires with radiative power larger than 100 MW as detected by VIIRS are indicated by the black dots. The VIIRS/NPP True color picture has been obtained via the NASA interactive platform EOSDIS Worldview (https://worldview.earthdata.nasa.gov/).

2×10^{16} mol.cm^{-2} and AAI > 3 for a total number of scenes of 60,000. Owing to its short lifetime, the high NO_2 condition ensures that the retained observations are located near intense emission sources while the AAI condition aims at excluding most of the anthropogenic pollution cases. In Figure 3, we examine the dependences of the CHOCHO and HCHO SCDs as well as R_{gf} on both the AAI and the injection height, using the effective scene pressure as a proxy. Panels (a) and (b) clearly show strong reductions of the CHOCHO SCD and R_{gf} for plumes located at higher altitudes (low pressures), while the dependence on AAI appears to be limited. The R_{gf} dependence closely follows the CHOCHO SCDs patterns, whereas the HCHO SCDs (panel c) slightly increase for low effective scene pressures. This small increase might be attributed to the expected increased sensitivity at higher altitudes. In addition, it indicates that the glyoxal depletion is not caused by a shielding effect as it can be reasonably assumed that different short-lived trace gases emitted by the same fires are located at approximately the same altitude. Panel (d) shows the overall dependence of the R_{gf} values on effective scene pressure. As indicated by the error bars representing the median absolute deviations, there is a large R_{gf} variability within each scene pressure bin related to the large range of sampled conditions. Nevertheless, the R_{gf} ratio shows a sharp decrease by a factor of 2–3 for scene pressures lower than 400 hPa compared to effective scenes closer to the ground. Note that this reduction derived from the global analysis is consistent with the corresponding reductions for the specific cases addressed in Section 3, as illustrated in Figure S3 in Supporting Information S1. In addition to Australia and California where the largest PyroCb events occurred, other world regions facing important fire events (e.g., Amazonia, Africa, Southeastern Asia, Siberia) contribute to the analysis (see Figure S4 in Supporting Information S1).

The strong reduction of R_{gf} over elevated fire plumes is not related to gas-phase sink processes (photolysis and reaction with OH), since the chemical lifetimes of HCHO and CHOCHO are similar, respectively about 4.6 and 3 hr on global average according to model simulations (Fu et al., 2008; Stavrakou et al., 2015). Furthermore, those losses are almost negligible within the time scale of the updraft (a few minutes), due to the extremely fast vertical velocities (>30 m s^{-1}) characterizing PyroCb clouds (Peterson et al., 2021). The observed glyoxal depletion is therefore likely caused by heterogeneous processes on aerosols or cloud droplets. Below the cloud base, the reactive uptake of glyoxal by aerosols is not expected to play an important role, in spite of the heavy smoke released by the fires, because the typical time scale for this sink exceeds 30 min, even for very large aerosol loadings (Kim et al., 2022). The negligible direct impact of aerosols is confirmed by the very weak

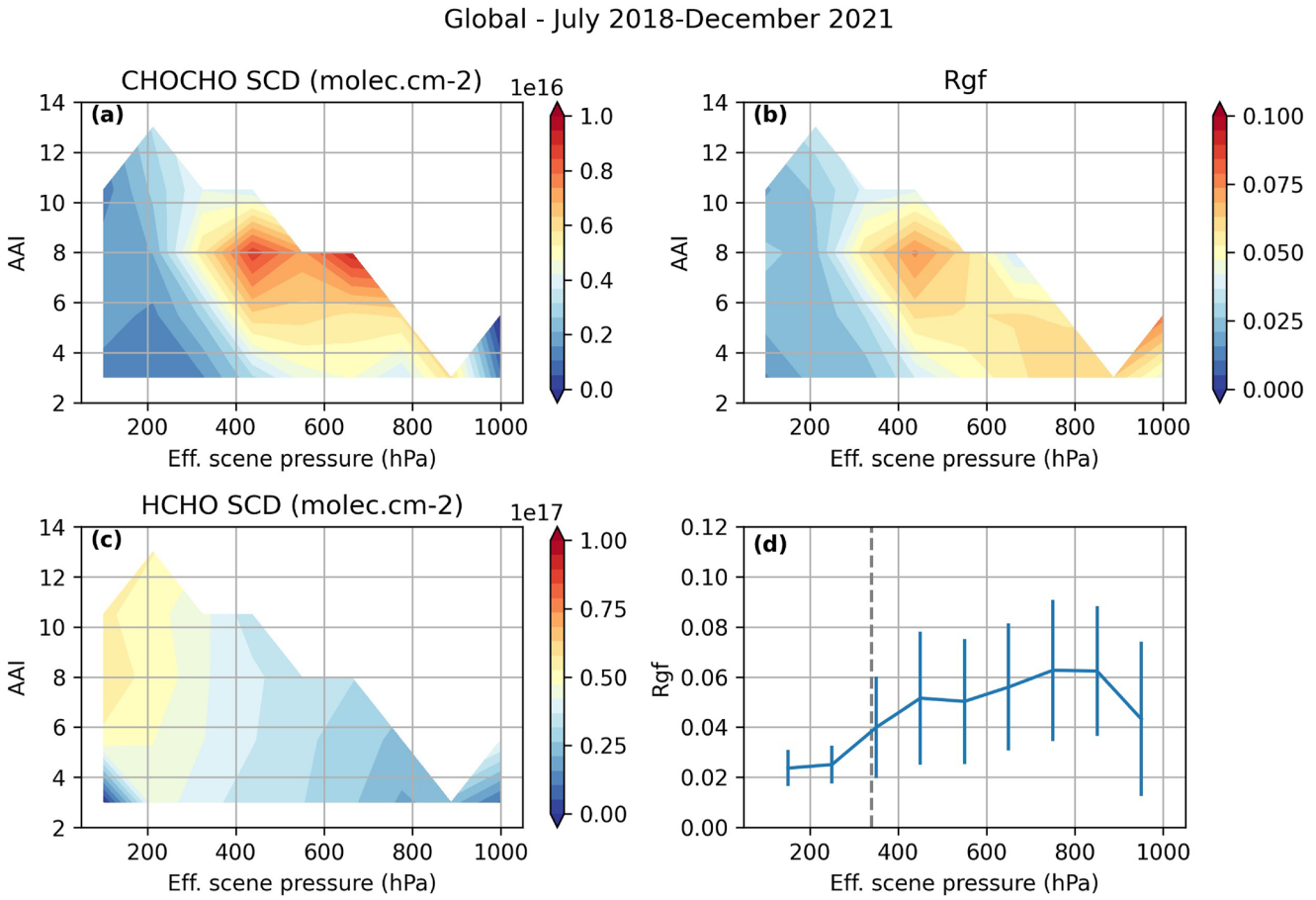

Figure 3. CHOCHO and HCHO SCDs (panels a–c) and derived glyoxal/formaldehyde ratio (panel b) as a function of the absorbing aerosol index (AAI) and effective scene pressure for all TROPOMI observations for which AAI > 3 and NO_2 SCD > 2×10^{16} mol.cm^{-2}, during July 2018–December 2021. Panel (d) shows the median R_{gf} as a function of the effective scene pressure, with the error bars representing the median absolute deviations. The dashed gray line indicates the typical freezing level.

dependence of R_{gf} on AAI for elevated plumes shown in Figure 3b. Above the cloud base, both formaldehyde and glyoxal partition between the gas and aqueous phases, owing to their Henry's law constant, respectively ~3.2×10^3 M atm^{-1} and ~4×10^5 M atm^{-1} at 298 K (Sander, 2015). In principle, both compounds can be washed out by precipitation. For example, scavenging efficiencies of the order of 50% were reported for HCHO during strong convection events at mid-latitudes (e.g., Fried et al., 2016), whereas lower values were estimated over West Africa (Borbon et al., 2012). Similar, or higher, scavenging efficiency is expected for glyoxal than for formaldehyde, due to its higher Henry's law constant. However, precipitation is strongly suppressed in PyroCb clouds, due to the unusually small droplet sizes caused by the massive presence of smoke particles, which are known to be very good cloud condensation nuclei (Andreae et al., 2004). The near-absence of precipitation precludes a significant role of wet scavenging and implies vigorous and efficient transport of water and pyrogenic emissions to upper levels. Another consequence of the small droplet sizes caused by the presence of smoke is that the PyroCb droplets remain mostly liquid up to the homogeneous freezing level (at about −38°C) (Rosenfeld et al., 2007), that is, in the upper troposphere. This might leave some room to aqueous chemistry in the PyroCb droplets, as (hydrated) glyoxal is known to react with OH in liquid water, producing organic acids and contributing to SOA formation (Ervens et al., 2004). However, this glyoxal sink is too slow, given current estimates of the OH-reaction rate constant (~10^9 M^{-1} s^{-1}) and the typical OH concentrations in cloud droplets (~10^{-13} M) (Ervens & Volkamer, 2010), corresponding to aqueous chemical lifetimes of several hours, much longer than the time required to reach the upper troposphere.

The absence of a noticeable depletion of formaldehyde slant columns for elevated plumes is consistent with previous observations of substantial enhancements of upper tropospheric HCHO due to deep convection (Fried

et al., 2016; Mari et al., 2000). The efficient upward transport of HCHO by deep convective clouds suggests that the irreversible sink of formaldehyde by outgassing of its hydrated form (methanediol - $CH_2(OH)_2$) from liquid cloud droplets, as proposed by Franco et al. (2021), does not play a very large role for such clouds, despite their large liquid water content, of the order of 2 g m^{-3} (Rosenfeld et al., 2007). At 280 K, ~40% of the HCHO would be present as (mostly aqueous-phase) methanediol in the warm part of the cloud, given its estimated Henry's law constant of 1.5×10^4 M atm^{-1} at that temperature (Sander, 2015). Whereas the remainder can reach the upper troposphere and contribute to the TROPOMI signal, the 40% loss of formaldehyde through methanediol formation is difficult to reconcile with the analysis of aircraft measurements by Fried et al. (2016) which required complete outgassing of formaldehyde from cloud droplets in order to explain the observations. Note that repeated cycles of evaporation/condensation would have the potential effect to further enhance the conversion of HCHO to methanediol. However, droplet evaporation was assumed by Franco et al. (2021) to be fast (<100 s), based on a modeling study of shallow convective clouds (Jarecka et al., 2013) characterized by very low cloud fractions (<8%). For large cloud systems such as PyroCb, extending typically over tens of km (e.g., Peterson et al., 2021), the droplet lifetime is usually much longer (Zung, 1967) and possibly exceeds the time required to reach the upper troposphere.

Regarding glyoxal, however, its pronounced depletion for cold clouds indicates that ice formation plays a key role, that is, either glyoxal remains largely in the condensed phase upon droplet freezing, or it is outgassed in hydrated form. Hydrated glyoxal does not have the characteristic absorption features of glyoxal and would not contribute to the glyoxal signal measured by the satellite. For plumes at lower altitudes, below the homogeneous freezing levels (−38°C/~340 hPa), R_{gf} is much less dependent on effective pressure. The large scatter associated to the R_{gf} estimates in those conditions makes the observed variability uncertain.

It is likely, but not certain, that the observed depletion of glyoxal occurs for other Cb types, for which droplet freezing starts at higher temperatures than in PyroCb clouds. Note that models generally assume zero retention efficiency for glyoxal, as for HCHO (Fu et al., 2008), despite the fact that high retention efficiencies were reported for other oxygenated VOCs such as methylhydroperoxide, CH_3OOH (Barth et al., 2016).

The direct consequences of these findings on the global budget of glyoxal are likely small. The low fraction (3%–5%) of the glyoxal global sink contributed by wet removal (Fu et al., 2008; Stavrakou et al., 2009) would be increased by a higher retention efficiency, since it would result in higher scavenging efficiencies in convective updrafts. On the other hand, hydrated glyoxal, if released, could be oxidized by OH or be taken up by clouds or aerosols, thereby enhancing SOA growth. Further research will be required to assess its potential impact in the atmosphere. A crucial question that warrants attention is the fate of methanediol trapped in liquid clouds, since its evaporation as either formaldehyde or its hydrate has very different consequences for the budget of formaldehyde and formic acid, which is the main product of methanediol oxidation by OH radicals (Franco et al., 2021). Further work will be needed to examine those processes in detail.

Data Availability Statement

TROPOMI CHOCHO data can be obtained via the GLYRETRO website (https://glyretro.aeronomie.be/index.php/data-menu-item/request-data-test). TROPOMI operational products used in this study (L2__HCHO__, L2__AER_AI, L2__NO2_) are publicly available via the ESA's S5P Pre-Ops interface (https://scihub.copernicus.eu/) using the credentials given there. The O_2-O_2 cloud parameters are contained in the NO_2 operational product. VIIRS FRP data have been retrieved from the Fire Information for Resource Management System (FIRMS) at https://firms.modaps.eosdis.nasa.gov/download/.

Acknowledgments
This work contains modified Copernicus Sentinel-5 Precursor satellite data (2018–2021). We acknowledge the use of imagery from the NASA Worldview application (https://worldview.earthdata.nasa.gov/), part of the NASA Earth Observing System Data and Information System (EOSDIS). Sérèna Docquier is gratefully acknowledged for her contribution to this work as part of her internship at BIRA-IASB.

References

Alvarado, L. M. A., Richter, A., Vrekoussis, M., Hilboll, A., Kalisz Hedegaard, A. B., Schneising, O., & Burrows, J. P. (2020). Unexpected long-range transport of glyoxal and formaldehyde observed from the Copernicus Sentinel-5 Precursor satellite during the 2018 Canadian wildfires. *Atmospheric Chemistry and Physics*, *20*(4), 2057–2072. https://doi.org/10.5194/acp-20-2057-2020

Andreae, M. O., Rosenfeld, D., Artaxo, P., Costa, A. A., Frank, G. P., Longo, K. M., & Silva-Dias, M. A. (2004). Smoking rain clouds over the Amazon. *Science*, *303*(5662), 1337–1342. https://doi.org/10.1126/science.1092779

Barth, M. C., Bela, M. M., Fried, A., Wennberg, P. O., Crounse, J. D., St. Clair, J. M., et al. (2016). Convective transport and scavenging of peroxides by thunderstorms observed over the Central U.S. during DC3. *Journal of Geophysical Research*, *121*(8), 4272–4295. https://doi.org/10.1002/2015JD024570

Borbon, A., Ruiz, M., Bechara, J., Aumont, B., Chong, M., Huntrieser, H., et al. (2012). Transport and chemistry of formaldehyde by mesoscale convective systems in West Africa during AMMA 2006. *Journal of Geophysical Research*, *117*(D12), D12301. https://doi.org/10.1029/2011JD017121

Byrne, B., Liu, J., Lee, M., Yin, Y., Bowman, K. W., Miyazaki, K., et al. (2021). The carbon cycle of southeast Australia during 2019–2020: Drought, fires, and subsequent recovery. *AGU Advances*, *2*(4). https://doi.org/10.1029/2021AV000469

Cao, H., Fu, T.-M., Zhang, L., Henze, D. K., Chan Miller, C., Lerot, C., et al. (2018). Adjoint inversion of Chinese non-methane volatile organic compound emissions using space-based observations of formaldehyde and glyoxal. *Atmospheric Chemistry and Physics*, *18*(20), 15017–15046. https://doi.org/10.5194/acp-18-15017-2018

Chang, D. Y., Yoon, J., Lelieveld, J., Park, S. K., Yum, S. S., Kim, J., & Jeong, S. (2021). Direct radiative forcing of biomass burning aerosols from the extensive Australian wildfires in 2019–2020. *Environmental Research Letters*, *16*(4), 044041. https://doi.org/10.1088/1748-9326/ABECFE

Chan Miller, C., Gonzalez Abad, G., Wang, H., Liu, X., Kurosu, T., Jacob, D. J., & Chance, K. (2014). Glyoxal retrieval from the ozone monitoring instrument. *Atmospheric Measurement Techniques*, *7*(11), 3891–3907. https://doi.org/10.5194/amt-7-3891-2014

Chimot, J., Pepijn Veefkind, J., de Haan, J. F., Stammes, P., & Levelt, P. F. (2019). Minimizing aerosol effects on the OMI tropospheric NO_2 retrieval—An improved use of the 477nm O_2-O_2 band and an estimation of the aerosol correction uncertainty. *Atmospheric Measurement Techniques*, *12*(1), 491–516. https://doi.org/10.5194/AMT-12-491-2019

Csiszar, I., Schroeder, W., Giglio, L., Ellicott, E., Vadrevu, K. P., Justice, C. O., & Wind, B. (2014). Active fires from the Suomi NPP visible infrared imaging radiometer suite: Product status and first evaluation results. *Journal of Geophysical Research: Atmospheres*, *119*(2), 803–816. https://doi.org/10.1002/2013JD020453

Damany-Pearce, L., Johnson, B., Wells, A., Osborne, M., Allan, J., Belcher, C., et al. (2022). Australian wildfires cause the largest stratospheric warming since Pinatubo and extends the lifetime of the Antarctic ozone hole. *Scientific Reports*, *12*(1), 1–15. https://doi.org/10.1038/s41598-022-15794-3

Das, S., Colarco, P. R., Oman, L. D., Taha, G., & Torres, O. (2021). The long-term transport and radiative impacts of the 2017 British Columbia pyrocumulonimbus smoke aerosols in the stratosphere. *Atmospheric Chemistry and Physics*, *21*(15), 12069–12090. https://doi.org/10.5194/ACP-21-12069-2021

De Smedt, I., Pinardi, G., Vigouroux, C., Compernolle, S., Bais, A., Benavent, N., et al. (2021). Comparative assessment of TROPOMI and OMI formaldehyde observations and validation against MAX-DOAS network column measurements. *Atmospheric Chemistry and Physics*, *21*(16), 12561–12593. https://doi.org/10.5194/ACP-21-12561-2021

di Virgilio, G., Evans, J. P., Blake, S. A. P., Armstrong, M., Dowdy, A. J., Sharples, J., & McRae, R. (2019). Climate change increases the potential for extreme wildfires. *Geophysical Research Letters*, *46*(14), 8517–8526. https://doi.org/10.1029/2019GL083699

Ervens, B., Feingold, G., Frost, G. J., & Kreidenweis, S. M. (2004). A modeling study of aqueous production of dicarboxylic acids: 1. Chemical pathways and speciated organic mass production. *Journal of Geophysical Research*, *109*(D15), D15205. https://doi.org/10.1029/2003JD004387

Ervens, B., & Volkamer, R. (2010). Glyoxal processing by aerosol multiphase chemistry: Towards a kinetic modeling framework of secondary organic aerosol formation in aqueous particles. *Atmospheric Chemistry and Physics*, *10*(17), 8219–8244. https://doi.org/10.5194/acp-10-8219-2010

Franco, B., Blumenstock, T., Cho, C., Clarisse, L., Clerbaux, C., Coheur, P.-F., et al. (2021). Ubiquitous atmospheric production of organic acids mediated by cloud droplets. *Nature*, *593*(7858), 233–237. https://doi.org/10.1038/s41586-021-03462-x

Fried, A., Barth, M. C., Bela, M., Weibring, P., Richter, D., Walega, J., et al. (2016). Convective transport of formaldehyde to the upper troposphere and lower stratosphere and associated scavenging in thunderstorms over the central United States during the 2012DC3 study. *Journal of Geophysical Research*, *121*(12), 7430–7460. https://doi.org/10.1002/2015JD024477

Fromm, M., Servranckx, R., Stocks, B. J., & Peterson, D. A. (2022). Understanding the critical elements of the pyrocumulonimbus storm sparked by high-intensity wildland fire. *Communications Earth & Environment*, *3*(243), 243. https://doi.org/10.1038/s43247-022-00566-8

Fu, T.-M. T.-M., Jacob, D. J., Wittrock, F., Burrows, J. P., Vrekoussis, M., & Henze, D. K. (2008). Global budgets of atmospheric glyoxal and methylglyoxal, and implications for formation of secondary organic aerosols. *Journal of Geophysical Research*, *113*(D15), D15303. https://doi.org/10.1029/2007JD009505

Galloway, M. M., Loza, C. L., Chhabra, P. S., Chan, A. W. H., Yee, L. D., Seinfeld, J. H., & Keutsch, F. N. (2011). Analysis of photochemical and dark glyoxal uptake: Implications for SOA formation. *Geophysical Research Letters*, *38*(17), 17811. https://doi.org/10.1029/2011GL048514

Grant, E., & Runkle, J. D. (2022). Long-term health effects of wildfire exposure: A scoping review. *The Journal of Climate Change and Health*, *6*, 100110. https://doi.org/10.1016/J.JOCLIM.2021.100110

Griffin, D., Mclinden, C. A., Dammers, E., Adams, C., Stockwell, C. E., Warneke, C., et al. (2021). Biomass burning nitrogen dioxide emissions derived from space with TROPOMI: Methodology and validation. *Atmospheric Measurement Techniques*, *14*(12), 7929–7957. https://doi.org/10.5194/amt-14-7929-2021

Hallquist, M., Wenger, J. C., Baltensperger, U., Rudich, Y., Simpson, D., Claeys, M., et al. (2009). The formation, properties and impact of secondary organic aerosol: Current and emerging issues. *Atmospheric Chemistry and Physics*, *9*(14), 5155–5236. https://doi.org/10.5194/acp-9-5155-2009

Hirsch, E., & Koren, I. (2021). Record-breaking aerosol levels explained by smoke injection into the stratosphere. *Science*, *371*(6535), 1269–1274. https://doi.org/10.1126/SCIENCE.ABE1415

Jarecka, D., Grabowski, W. W., Morrison, H., & Pawlowska, H. (2013). Homogeneity of the subgrid-scale turbulent mixing in large-eddy simulation of shallow convection. *Journal of the Atmospheric Sciences*, *70*(9), 2751–2767. https://doi.org/10.1175/JAS-D-13-042.1

Jiang, Y., Lu, Z., Liu, X., Qian, Y., Zhang, K., Wang, Y., & Yang, X. Q. (2016). Impacts of global open-fire aerosols on direct radiative, cloud and surface-albedo effects simulated with CAM5. *Atmospheric Chemistry and Physics*, *16*(23), 14805–14824. https://doi.org/10.5194/ACP-16-14805-2016

Jin, X., Zhu, Q., Cohen, R. C., & Xiaomeng, J. (2021). Direct estimates of biomass burning NO_x emissions and lifetimes using daily observations from TROPOMI. *Atmospheric Chemistry and Physics*, *21*(20), 15569–15587. https://doi.org/10.5194/acp-21-15569-2021

Johnson, M. S., Strawbridge, K., Knowland, K. E., Keller, C., & Travis, M. (2021). Long-range transport of Siberian biomass burning emissions to North America during FIREX-AQ. *Atmospheric Environment*, *252*, 118241. https://doi.org/10.1016/J.ATMOSENV.2021.118241

Kaiser, J., Wolfe, G. M., Min, K. E., Brown, S. S., Miller, C. C., Jacob, D. J., et al. (2015). Reassessing the ratio of glyoxal to formaldehyde as an indicator of hydrocarbon precursor speciation. *Atmospheric Chemistry and Physics*, *15*(13), 7571–7583. https://doi.org/10.5194/acp-15-7571-2015

Kim, D., Cho, C., Jeong, S., Lee, S., Nault, B. A., Camuzano-Jost, P., et al. (2022). Field observational constraints on the controllers in glyoxal (CHOCHO) reactive uptake to aerosol. *Atmospheric Chemistry and Physics*, *22*(2), 805–821. https://doi.org/10.5194/acp-22-805-2022

Kloss, C., Sellitto, P., von Hobe, M., Berthet, G., Smale, D., Krysztofiak, G., et al. (2021). Australian fires 2019–2020: Tropospheric and stratospheric pollution throughout the whole fire season. *Frontiers in Environmental Science*, *9*, 220. https://doi.org/10.3389/FENVS.2021.652024/BIBTEX

Kluge, F., Hüneke, T., Knecht, M., Lichtenstern, M., Rotermund, M., Schlager, H., et al. (2020). Profiling of formaldehyde, glyoxal, methylglyoxal, and CO over the Amazon: Normalized excess mixing ratios and related emission factors in biomass burning plumes. *Atmospheric Chemistry and Physics*, *20*(20), 12363–12389. https://doi.org/10.5194/acp-20-12363-2020

Knote, C., Hodzic, A., Jimenez, J. L., Volkamer, R., Orlando, J. J., Baidar, S., et al. (2014). Simulation of semi-explicit mechanisms of SOA formation from glyoxal in aerosol in a 3-D model. *Atmospheric Chemistry and Physics*, *14*(12), 6213–6239. https://doi.org/10.5194/acp-14-6213-2014

Lareau, N. P., Nauslar, N. J., Bentley, E., Roberts, M., Emmerson, S., Brong, B., et al. (2022). Fire-generated tornadic vortices. *Bulletin of the American Meteorological Society*, *103*(5), E1296–E1320. https://doi.org/10.1175/BAMS-D-21-0199.1

Lerot, C., Hendrick, F., Van Roozendael, M., Alvarado, L. M. A., Richter, A., De Smedt, I., et al. (2021). Glyoxal tropospheric column retrievals from TROPOMI—Multi-satellite intercomparison and ground-based validation. *Atmospheric Measurement Techniques*, *14*(12), 7775–7807. https://doi.org/10.5194/AMT-14-7775-2021

Li, F., Zhang, X., Kondragunta, S., & Lu, X. (2020). An evaluation of advanced baseline imager fire radiative power based wildfire emissions using carbon monoxide observed by the Tropospheric Monitoring Instrument across the conterminous United States. *Environmental Research Letters*, *15*(9), 094049. https://doi.org/10.1088/1748-9326/AB9D3A

Li, J., Mao, J., Min, K.-E., Washenfelder, R. A., Brown, S. S., Kaiser, J., et al. (2016). Observational constraints on glyoxal production from isoprene oxidation and its contribution to organic aerosol over the Southeast United States. *Journal of Geophysical Research: Atmospheres*, *121*(16), 9849–9861. https://doi.org/10.1002/2016JD025331

Magro, C., Nunes, L., Gonçalves, O. C., Neng, N. R., Nogueira, J. M. F., Rego, F. C., & Vieira, P. (2021). Atmospheric trends of CO and CH_4 from extreme wildfires in Portugal using Sentinel-5P TROPOMI level-2 data. https://doi.org/10.3390/fire4020025

Majdi, M., Sartelet, K., Maria Lanzafame, G., Couvidat, F., Kim, Y., Chrit, M., & Turquety, S. (2019). Precursors and formation of secondary organic aerosols from wildfires in the Euro-Mediterranean region. *Atmospheric Chemistry and Physics*, *19*(8), 5543–5569. https://doi.org/10.5194/ACP-19-5543-2019

Mari, C., Jacob, D. J., & Bechtold, P. (2000). Transport and scavenging of soluble gases in a deep convective cloud. *Journal of Geophysical Research*, *105*(D17), 22255–22267. https://doi.org/10.1029/2000JD900211

Miao, R., Chen, Q., Shrivastava, M., Chen, Y., Zhang, L., Hu, J., et al. (2021). Process-based and observation-constrained SOA simulations in China: The role of semivolatile and intermediate-volatility organic compounds and OH levels. *Atmospheric Chemistry and Physics*, *21*(21), 16183–16201. https://doi.org/10.5194/ACP-21-16183-2021

Nolan, R. H., Bowman, D. M. J. S., Clarke, H., Haynes, K., Ooi, M. K. J., Price, O. F., et al. (2021). What do the Australian black summer fires signify for the global fire crisis? *Fire*, *4*(4), 97. https://doi.org/10.3390/FIRE4040097/S1

Oak, Y. J., Park, R. J., Jo, D. S., Hodzic, A., Jimenez, J. L., Campuzano-Jost, P., et al. (2022). Evaluation of secondary organic aerosol (SOA) simulations for seoul, Korea. *Journal of Advances in Modeling Earth Systems*, *14*(2), e2021MS002760. https://doi.org/10.1029/2021MS002760

Pai, S. J., Heald, C. L., Pierce, J. R., Farina, S. C., Marais, E. A., Jimenez, J. L., et al. (2020). An evaluation of global organic aerosol schemes using airborne observations. *Atmospheric Chemistry and Physics*, *20*(5), 2637–2665. https://doi.org/10.5194/ACP-20-2637-2020

Palm, B. B., Peng, Q., Fredrickson, C. D., Lee, B. H., Garofalo, L. A., Pothier, M. A., et al. (2020). Quantification of organic aerosol and Brown carbon evolution in fresh wildfire plumes. *Proceedings of the National Academy of Sciences of the United States of America*, *117*, 29469–29477. https://doi.org/10.1073/PNAS.2012218117/SUPPL_FILE/PNAS.2012218117.SD01

Pausas, J. G., & Keeley, J. E. (2021). Wildfires and global change. *Frontiers in Ecology and the Environment*, *19*(7), 387–395. https://doi.org/10.1002/FEE.2359

Pennington, E. A., Seltzer, K. M., Murphy, B. N., Qin, M., Seinfeld, J. H., & Pye, H. O. T. (2021). Modeling secondary organic aerosol formation from volatile chemical products. *Atmospheric Chemistry and Physics*, *21*(24), 18247–18261. https://doi.org/10.5194/ACP-21-18247-2021

Peterson, D. A., Fromm, M. D., McRae, R. H. D., Campbell, J. R., Hyer, E. J., Taha, G., et al. (2021). Australia's Black Summer pyrocumulonimbus super outbreak reveals potential for increasingly extreme stratospheric smoke events. *Npj Climate and Atmospheric Science*, *4*(1), 1–16. https://doi.org/10.1038/s41612-021-00192-9

Platt, U., & Stutz, J. (2008). *Differential optical absorption spectroscopy: Principles and applications*. Springer-Verlag.

Rosenfeld, D., Fromm, M., Trentmann, J., Luderer, G., Andreae, M. O., & Servranckx, R. (2007). The chisholm firestorm: Observed microstructure, precipitation and lightning activity of a pyro-cumulonimbus. *Atmospheric Chemistry and Physics*, *7*(3), 645–659. https://doi.org/10.5194/acp-7-645-2007

Ryan, R. G., Silver, J. D., & Schofield, R. (2021). Air quality and health impact of 2019–20 Black Summer megafires and COVID-19 lockdown in Melbourne and Sydney, Australia. *Environmental Pollution*, *274*, 116498. https://doi.org/10.1016/J.ENVPOL.2021.116498

Sander, R. (2015). Compilation of Henry's law constants (version 4.0) for water as solvent. *Atmospheric Chemistry and Physics*, *15*(8), 4399–4981. https://doi.org/10.5194/acp-15-4399-2015

Schwartz, M. J., Santee, M. L., Pumphrey, H. C., Manney, G. L., Lambert, A., Livesey, N. J., et al. (2020). Australian new year's PyroCb impact on stratospheric composition. *Geophysical Research Letters*, *47*(24), e2020GL090831. https://doi.org/10.1029/2020GL090831

Senande-Rivera, M., Insua-Costa, D., & Miguez-Macho, G. (2022). Spatial and temporal expansion of global wildland fire activity in response to climate change. *Nature Communications*, *13*(1), 1–9. https://doi.org/10.1038/s41467-022-28835-2

Solomon, S., Dube, K., Stone, K., Yu, P., Kinnison, D., Toon, O. B., et al. (2022). On the stratospheric chemistry of midlatitude wildfire smoke. *Proceedings of the National Academy of Sciences of the United States of America*, *119*, e2117325119. https://doi.org/10.1073/PNAS.2117325119/SUPPL_FILE/PNAS.2117325119

Stavrakou, T., Müller, J.-F., Bauwens, M., De Smedt, I., Van Roozendael, M., De Mazière, M., et al. (2015). How consistent are top-down hydrocarbon emissions based on formaldehyde observations from GOME-2 and OMI? *Atmospheric Chemistry and Physics*, *15*(20), 11861–11884. https://doi.org/10.5194/acp-15-11861-2015

Stavrakou, T., Müller, J.-F., de Smedt, I., van Roozendael, M., Kanakidou, M., Vrekoussis, M., et al. (2009). The continental source of glyoxal estimated by the synergistic use of spaceborne measurements and inverse modelling. *Atmospheric Chemistry and Physics*, *9*(21), 8431–8446. https://doi.org/10.5194/acp-9-8431-2009

Stein Zweers, D. C. (2022). TROPOMI ATBD of the UV aerosol. 2.1.0. Retrieved from https://sentinel.esa.int/documents/247904/0/Sentinel-5P-TROPOMI-ATBD-UV-Aerosol-Index/b2fe35ff-9a53-4970-a3e6-d09319c89083

Theys, N., Volkamer, R., Müller, J. F., Zarzana, K. J., Kille, N., Clarisse, L., et al. (2020). Global nitrous acid emissions and levels of regional oxidants enhanced by wildfires. *Nature Geoscience*, *13*(10), 681–686. https://doi.org/10.1038/s41561-020-0637-7

van der Velde, I. R., van der Werf, G. R., Houweling, S., Eskes, H. J., Pepijn Veefkind, J., Borsdorff, T., & Aben, I. (2021). Biomass burning combustion efficiency observed from space using measurements of CO and NO_2 by the TROPOspheric Monitoring Instrument (TROPOMI). *Atmospheric Chemistry and Physics*, *21*(2), 597–616. https://doi.org/10.5194/ACP-21-597-2021

van der Velde, I. R., van der Werf, G. R., Houweling, S., Maasakkers, J. D., Borsdorff, T., Landgraf, J., et al. (2021). Vast CO_2 release from Australian fires in 2019–2020 constrained by satellite. *Nature*, *597*(7876), 366–369. https://doi.org/10.1038/s41586-021-03712-y

van Geffen, J., Eskes, H., Compernolle, S., Pinardi, G., Verhoelst, T., Lambert, J. C., et al. (2022). Sentinel-5P TROPOMI NO_2 retrieval: Impact of version v2.2 improvements and comparisons with OMI and ground-based data. *Atmospheric Measurement Techniques*, *15*(7), 2037–2060. https://doi.org/10.5194/AMT-15-2037-2022

Veefkind, J. P., Aben, I., McMullan, K., Förster, H., de Vries, J., Otter, G., et al. (2012). TROPOMI on the ESA Sentinel-5 precursor: A GMES mission for global observations of the atmospheric composition for climate, air quality and ozone layer applications. *Remote Sensing of Environment*, *120*, 70–83. https://doi.org/10.1016/j.rse.2011.09.027

Veefkind, P. J., de Haan, J. F., Sneep, M., & Levelt, P. F. (2016). Improvements to the OMI O_2-O_2 operational cloud algorithm and comparisons with ground-based radar-lidar observations. *Atmospheric Measurement Techniques*, *9*(12), 6035–6049. https://doi.org/10.5194/amt-9-6035-2016

Volkamer, R., San Martini, F., Molina, L. T., Salcedo, D., Jimenez, J. L., & Molina, M. J. (2007). A missing sink for gas-phase glyoxal in Mexico City: Formation of secondary organic aerosol. *Geophysical Research Letters*, *34*(19), L19807. https://doi.org/10.1029/2007GL030752

Voulgarakis, A., & Field, R. D. (2015). Fire influences on atmospheric composition, air quality and climate. *Current Pollution Reports*, *1*(2), 70–81. https://doi.org/10.1007/S40726-015-0007-Z

Vrekoussis, M., Wittrock, F., Richter, A., & Burrows, J. P. (2010). GOME-2 observations of oxygenated VOCs: What can we learn from the ratio glyoxal to formaldehyde on a global scale? *Atmospheric Chemistry and Physics*, *10*(21), 10145–10160. https://doi.org/10.5194/acp-10-10145-2010

Wang, P., Tuinder, O. N. E., Tilstra, L. G., de Graaf, M., & Stammes, P. (2012). Interpretation of FRESCO cloud retrievals in case of absorbing aerosol events. *Atmospheric Chemistry and Physics*, *12*(19), 9057–9077. https://doi.org/10.5194/ACP-12-9057-2012

Xu, R., Yu, P., Abramson, M. J., Johnston, F. H., Samet, J. M., Bell, M. L., et al. (2020). Wildfires, global climate change, and human health. *New England Journal of Medicine*, *383*(22), 2173–2181. https://doi.org/10.1056/NEJMSR2028985/SUPPL_FILE/NEJMSR2028985_DISCLOSURES.PDF

Zarzana, K. J., Selimovic, V., Koss, A. R., Sekimoto, K., Coggon, M. M., Yuan, B., et al. (2018). Primary emissions of glyoxal and methylglyoxal from laboratory measurements of open biomass burning. *Atmospheric Chemistry and Physics*, *18*(20), 15451–15470. https://doi.org/10.5194/ACP-18-15451-2018

Zung, J. T. (1967). Evaporation rate and lifetimes of clouds and sprays in air—The cellular model. *Journal of Chemical Physics*, *46*(6), 2064–2070. https://doi.org/10.1063/1.1841002